Inorganic Chemistry

Article

Cite This: Inorg. Chem. 2017, 56, 13293-13299

pubs.acs.org/IC

Artificial Metalloproteins for Binding and Stabilization of a Semiquinone Radical

Nathalie Ségaud, Ivana Drienovská, Juan Chen, Wesley R. Browne, and Gerard Roelfes*

Stratingh Institute for Chemistry, University of Groningen, Nijenborgh 4, 9747 AG Groningen, The Netherlands

Supporting Information

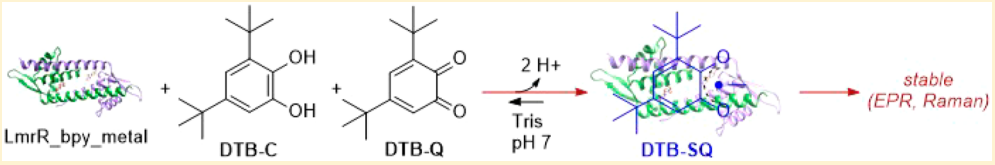

ABSTRACT: The interaction of a number of first-row transition-metal ions with a 2,2′-bipyridyl alanine (bpyA) unit incorporated into the lactococcal multidrug resistance regulator (LmrR) scaffold is reported. The composition of the active site is shown to influence binding affinities. In the case of Fe(II), we demonstrate the need of additional ligating residues, in particular those containing carboxylate groups, in the vicinity of the binding site. Moreover, stabilization of di-*tert*-butylsemiquinone radical (**DTB-SQ**) in water was achieved by binding to the designed metalloproteins, which resulted in the radical being shielded from the aqueous environment. This allowed the first characterization of the radical semiquinone in water by resonance Raman spectroscopy.

INTRODUCTION

Artificial metalloenzymes have emerged as a promising strategy to emulate the catalytic efficiency of natural metalloenzymes in new to nature reactions.[1−12] In addition to their potential for application in synthesis, they are also valuable tools for the investigation of the role of the second coordination sphere in enzyme catalysis.[3,13−18] Furthermore, designed metalloproteins may allow for the stabilization of highly reactive compounds, giving rise to increased lifetimes of these species. Some metal semiquinone intermediates have been identified in natural enzymes and synthetic mimic complexes.[19,20] In one such example, DeGrado et al. recently reported the stabilization of the radical 3,5-di-*tert*-butylsemiquinone (**DTB-SQ**), which results from the one-electron oxidation of 3,5-di-*tert*-butylcatechol (**DTB-C**) (Scheme 1), in the interior of a de novo designed metalloprotein [DFsc-Zn^{II}_2].[21] *o*-Semiquinones are important radicals that natural metalloenzymes generate inside their pocket during the catalytic oxidation of catechols to quinones or in the oxidative cleavage of catechols.[22−24] Notably, **DTB-SQ** rapidly decomposes in an aqueous environment; however, the coordination to zinc ions allows the radical to bind in the hydrophobic environment provided by DFsc and it is thus shielded from bulk water.

We have developed a class of artificial metalloenzymes based on multidrug resistance regulators such as the transcription factor lactococcal multidrug resistance regulator (LmrR).[25−29] This homodimeric protein has a large hydrophobic pocket at the dimer interface that has proven suitable for the creation of novel active sites. Recently, we have reported the introduction of the metal-binding unnatural amino acid 2,2′-bipyridyl alanine (bpyA) in LmrR using stop codon suppression methodology (Figure 1).[30] Upon binding of Cu(II) ions, the resulting artificial metalloenzymes were then employed successfully in Friedel−Crafts alkylation reactions.[25]

Scheme 1. Redox Chemistry and Formation of the Radical Anion DTB-SQ at pH 7: (a) Comproportionation between Catechol DTB-C and Quinone DTB-Q; (b) Two-Electron Oxidation of DTB-C to DTB-Q, Where the One-Electron-Oxidized Product Is DTB-SQ

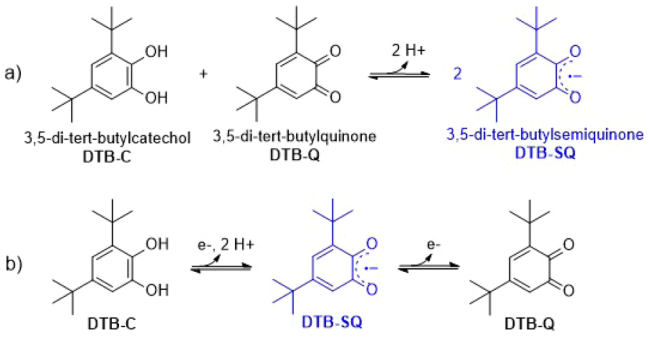

Here we report on the coordination chemistry of a variety of LmrR-based metalloproteins, involving different metal ions, and the binding and stabilization of *o*-semiquinone radicals.

RESULTS AND DISCUSSION

On the basis of X-ray crystal structures and our earlier studies,[25,31,32] positions situated at the ends of the protein pocket were selected for the introduction of bpyA within the hydrophobic environment: positions V15, N19, and M89.

Received: August 12, 2017
Published: October 13, 2017

DOI: 10.1021/acs.inorgchem.7b02073
Inorg. Chem. 2017, 56, 13293−13299

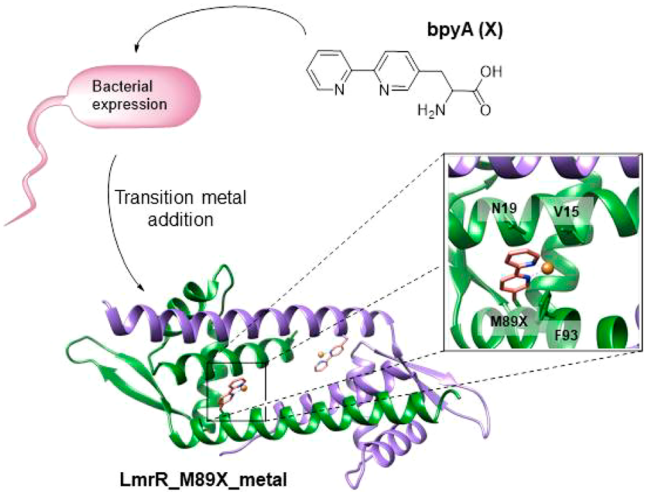

Figure 1. In vivo incorporation of bpyA (X) into LmrR protein and metal binding, with a detailed picture of the modeled binding site of LmrR_M89X.

LmrR is homodimeric, and it is important to note that every protein contains two bpyA residues in the hydrophobic pocket: one from each monomer. In the case of the mutant LmrR_M89X, positions V15 and F93, which are spatially close to the bpyA residue at position 89, were mutated to introduce additional dative ligands for the metal ion: i.e., carboxylate and imidazole moieties. These mutations were envisioned to result in binding sites that mimic the 2His-1 Carboxylate triad often found in nonheme iron proteins[33] and the 3His motif observed in Zn(II) proteins.[34] The different mutants were expressed, purified, and characterized as previously reported (see the Supporting Information).[25]

Metal Ion Binding. In our earlier report, Cu(II) binding to LmrR_M89X resulted in a 1:1 metal to LmrR monomer ratio.[25] In the present study, we expanded the investigation of the coordination chemistry of this artificial metalloprotein to other first-row transition-metal ions: Mn(II), Fe(II), Co(II), Ni(II), and Zn(II).

The bpyA unnatural amino acid itself showed binding of all the studied metal ions under neutral aqueous conditions (Figure S3 in the Supporting Information). Binding of the metal ions is manifested in a shift of the ligand $\pi-\pi^*$ transition UV absorption band (280−310 nm).[35,36] The K_d values and metal to bpyA ratios were determined from a titration curve with fitting of absorbance at 305 nm (Table 1 and Table S2 in the Supporting Information) and revealed the highest affinities for Cu(II) and Fe(II) and the lowest for Zn(II). In the case of Mn(II), a more complicated behavior was observed (vide infra).

With LmrR_M89X, binding of Co(II), Ni(II), Cu(II), and Zn(II) was manifested in the absorption band at 310 nm, assigned to the $\pi-\pi^*$ transition from the bipyridyl (bpy) moiety in bpy-metal complexes (Figure 2 and Figure S4 in the Supporting Information). Cu(II) and Ni(II) showed a 1:1 metal to protein monomer ratio and low K_d values (<0.1 μM, Table S3 in the Supporting Information) that are 1−2 orders of magnitude lower than those reported for bpyA-containing peptides (8 μM for Cu(II) and 50 μM for Ni(II)),[37] showing the favorable contribution of the protein environment to metal ion binding. In case of Co(II) and Zn(II) ions, the protein precipitated upon addition of ≥1 equiv of metal salt with respect to monomer. Finally, during titration of Fe(II) and Mn(II), changes in the absorption spectra were not observed, indicating that these metal ions are not binding.

Table 1. Dissociation Constants, Molar Absorptivities, and Metal Ion to Binding Site Ratios for the Different Metal Ions Determined with bpyA and LmrR Mutants

ligand/protein	metal ion	K_d (μM)	ratio	ε (cm^{-1} M^{-1})
bpyA	Fe(II)	0.18 ± 0.18	1:2	27100
	Cu(II)	0.00 ± 0.00	1:1	11690
	Zn(II)	5.85 ± 0.95	1:2	23930
	Co(II)	1.45 ± 0.82	1:3	32960
	Ni(II)	0.49 ± 0.21	1:3	32840
M89X	Cu(II)	0.04 ± 0.05	1:1	15770
	Ni(II)	0.05 ± 0.06	1:1	16410
M89X_	Fe(II)	1.67 ± 0.93	1:1	13850
V15E_	Cu(II)	0.31 ± 0.08	1:1	14050
F93D	Zn(II)	0.84 ± 0.39	1:1	12480
	Ni(II)	0.65 ± 0.07	1:2	26390
V15X	Zn(II)	1.35 ± 0.59	1:1	4120
N19X	Zn(II)	1.52 ± 0.33	1:1	10660
M89X_F93D	Zn(II)	0.28 ± 0.07	1:1	13290
M89X_F93H	Zn(II)	1.41 ± 0.51	1:1	14080
M89X_V15H_F93H	Zn(II)	1.75 ± 0.38	1:1	11670

In an attempt to improve the binding of these metal ions, mutations at positions V15 and F93, which are in the vicinity of the bpyA residue, to carboxylate- or imidazole-containing residues were evaluated. In the case of histidine mutation at position F93, the absorption spectrum of LmrR_M89X_F93H was unaffected in the presence of Fe(II); thus, its coordination was not observed. In contrast, mutation of this position to aspartate, i.e. LmrR_M89X_F93D, did result in coordination of Fe(II), as suggested by the appearance of the 310 nm band in the absorption spectrum (Figure S5 in the Supporting Information). However, the titration curve with Fe(II) was not well-defined. Therefore, an additional carboxylate moiety was added to the coordination sphere by mutation of position V15 to glutamate: i.e., LmrR_M89X_V15E_F93D. With these additional dative ligands present, Fe(II) binding was observed, as evidenced by the appearance of the 310 nm absorption band and a well-defined titration curve, analysis of which showed a 1:1 metal ion to protein monomer binding ratio and a K_d value of 1.67 μM (Figure S6 in the Supporting Information). Hence, it can be concluded that additional carboxylato ligands are important for achieving Fe(II) binding to the bpy moiety, likely by mimicking the 2 His-1Carboxylate triad in the active site of natural Fe(II) enzymes. However, also with this mutant, Mn(II) coordination was still not observed.

The binding of the other metal ions to LmrR_M89X_V15E_F93D was investigated (Figure S7 and Table S4 in the Supporting Information) and this indicated that the mutations did not benefit Cu(II) and Ni(II) binding, with K_d values similar to those with LmrR_M89X: i.e., 0.3 and 0.65 μM, respectively (Table 1). The metal to monomer ratios were estimated to be 1:1 for Fe(II), Cu(II), and Zn(II), which correspond to the ratios established with LmrR_M89X. Interestingly, a 1:2 metal binding ratio was determined for Ni(II), which indicates that the coordination is different in LmrR_M89X in comparison to M89X_V15E_F93D. With Co(II), again precipitation was observed after addition of more than 1 equiv.

The influence of the position of bpyA on metal ion binding was studied with Zn(II) and the mutants LmrR_V15X and

DOI: 10.1021/acs.inorgchem.7b02073
Inorg. Chem. 2017, 56, 13293−13299

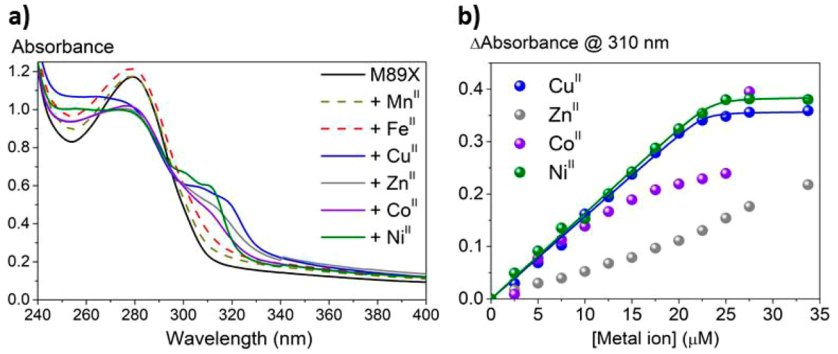

Figure 2. (a) UV absorption spectra of 30 μM monomer LmrR_M89X in the presence of 1 equiv of metal ion. (b) Absorption at 310 nm with increasing amounts of metal ions and curve fitting (fitting values in Table S3 in the Supporting Information).

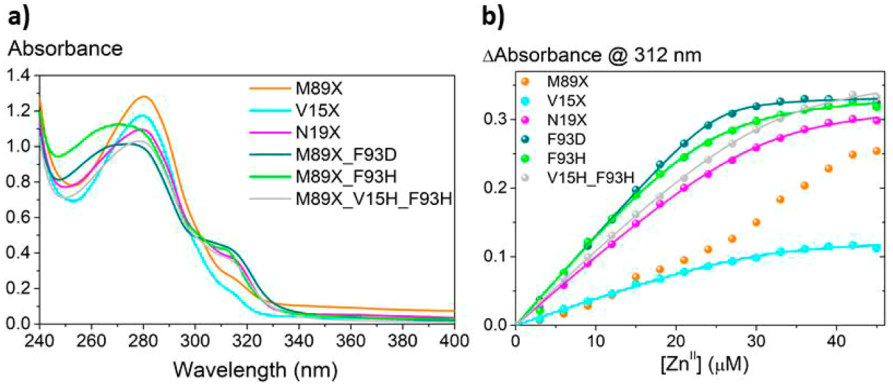

Figure 3. (a) UV absorption spectra of 30 μM monomer LmrR mutants in the presence of 1 equiv of Zn(II). (b) Absorption at 312 nm with addition of Zn(II) and curve fitting (fitting values in Table S5 in the Supporting Information).

N19X. In contrast to LmrR_M89X, well-defined behavior was observed with 1:1 metal to monomer ratios and low micromolar K_d values (Figure 3 and Figure S8 in the Supporting Information). Interestingly, the molar absorptivities were almost twice as high for LmrR_N19X than for LmrR_V15X. The K_d values were found to be comparable to that measured for LmrR_M89X_V15E_F93D (Table 1 and Table S5 in the Supporting Information). Thus, in contrast to LmrR_M89X, the proteins with bpyA at positions V15 and N19 do provide a good binding environment for Zn(II), which may be due to carboxylate ligands from D100 and E104 that are present in the vicinity (Figure S9 in the Supporting Information).

Finally, the influence of additional ligating residues in the vicinity of the M89X residue on Zn(II) binding was investigated for LmrR_M89X mutants. As previously mentioned, mutant M89X_V15E_F93D improved the binding of Zn(II). M89X_F93D, M89X_F93H, and M89X_V15H_F93H were prepared to provide carboxylate or imidazole groups, in order to complete the zinc coordination sphere.[38] With all three mutants, formation of the band around 310 nm was observed and 1:1 metal to monomer ratios were determined (Figure 3 and Figure S8 in the Supporting Information). The lowest K_d value was determined for M89X_F93D (0.28 μM, Table 1 and Table S5 in the Supporting Information), which was 1 order of magnitude lower than those obtained for the histidine mutants.

UV−Vis Absorption Spectroscopy of Binding of DTB-SQ. The semiquinone anion radical **DTB-SQ** was generated in aqueous medium by comproportionation between the catechol **DTB-C** and the quinone **DTB-Q** (Scheme 1). In aqueous media, only two-electron oxidation/reduction is observed and the semiquinone radical has not been detected;[39] a hydrophobic environment is thus essential to isolate it from water and stabilize it.

LmrR_M89X, without added metal ion, shows no ability to stabilize **DTB-SQ**: i.e., spectral features are not observed by UV−vis absorption and electron paramagnetic spectroscopy, indicating that no radical species was detected. In the presence of 0.9 equiv of metal ion (Cu(II), Zn(II), Co(II), and Ni(II)) with respect to the concentration in protein monomer, two absorption bands were observed in the near-IR region of the spectra (Figure 4, Figure S10 in the Supporting Information, and Table 2), although they are only weak for Co(II). These bands are similar to those observed with the designed metalloprotein [DFsc-Zn$^{II}_2$] and, hence, are assigned to the

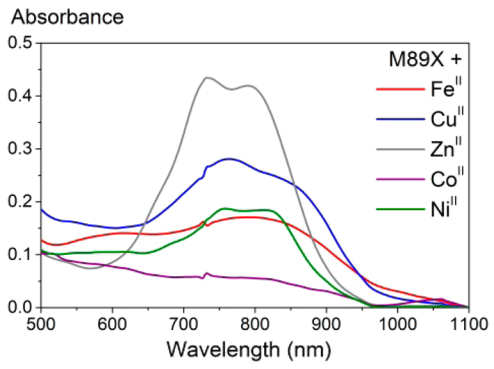

Figure 4. Vis−NIR absorption spectra of LmrR_M89X 30 μM + 0.9 equiv of metal ion + 300 μM **DTB-C**:**DTB-Q** (1:1) after 24 h.

DOI: 10.1021/acs.inorgchem.7b02073
Inorg. Chem. 2017, 56, 13293−13299

Table 2. Absorbance Maxima of DTB-SQ Absorption Band Measured with LmrR_M89X and LmrR_M89X_V15E_F93D, in the Presence of Transition-Metal Ions

	M89X		M89X_V15E_F93D	
	$\lambda_{max}(1)$ (nm)	$\lambda_{max}(2)$ (nm)	$\lambda_{max}(1)$ (nm)	$\lambda_{max}(2)$ (nm)
Cu(II)	764	~850	765	~850
Zn(II)	739	789	733	801
Co(II)	733	780	732	788
Ni(II)	758	813	764	817
Fe(II)[a]	n.d.	n.d.	745	803

[a]Protein incubated with an excess of Fe(II) followed by dialysis to remove the excess of metal ions.

radical semiquinone **DTB-SQ** (vide infra).[21] The differences in absorbance are due to different yields in **DTB-SQ**, as observed by resonance Raman spectroscopy (vide infra). In comparison to Zn(II), about half the **DTB-SQ** is obtained with Cu(II) and Ni(II) and only 20% with Co(II). Attempts to determine the kinetics of semiquinone radical formation for the various metalloproteins were unsuccessful, which might be due to other processes such as binding being rate limiting.

In the presence of Fe(II), a different behavior was observed. While in the absence of **DTB-C** binding of Fe(II) was not observed (vide supra), two broad absorption bands centered at 790 and 617 nm were observed when **DTB-C** was present. However, this is characteristic for an Fe(III)-catecholate species, reminiscent of the intermediate identified in catechol oxidases.[22] Such catecholate model complexes have been reported based on aminopyridine ligands, with two bands in the visible (500−580 nm) and NIR (800−950 nm) regions of their absorption spectra in organic solvent.[40−42] Moreover, the absorption spectrum of $[Fe^{III}(cat)_3]^{3+}$ in water shows only one band at 570 nm.[19] The spectrum observed for LmrR_M89X in the presence of Fe(II) and **DTB-C** suggests that a bpy-Fe(III)-catecholato complex is generated under aerobic conditions, and catechol cleavage does not occur.

Similar behavior was observed with LmrR_M89X_V15E_F93D in the presence of 0.9 equiv of the different metal ions (Figure S11 in the Supporting Information). An Fe(III)-catecholato species was predominantly formed with Fe(II), while **DTB-SQ** was detected with similar yields for the other metal ions. The absorbance maxima for the radical semiquinone absorption band were mainly red shifted in comparison to those measured with LmrR_M89X (Table 2), most probably due to the different binding environment offered by LmrR_ M89X_V15E_F93D.

In an alternative approach, LmrR_M89X_V15D_F93D_Fe(II) was prepared by incubation with excess Fe(II) followed by dialysis to remove the excess of metal ion. Upon addition of **DTB-C**/**DTB-Q**, absorption bands centered at 745 and 803 nm were observed, indicative of **DTB-SQ** (Figure S12 in the Supporting Information and Table 2). In this case, a band at 614 nm was not observed, suggesting that the Fe(III)-catecholato species was not generated under these conditions. Thus, removal of free Fe(II) ions avoids the formation of Fe(III)-catecholate and only the radical semiquinone is observed.

The importance of the position of the binding site was determined for the Zn(II)-containing proteins (Figure S13 in the Supporting Information). All artificial zinc proteins showed absorption bands typical for **DTB-SQ**, although shifts in absorbance maxima of the **DTB-SQ** absorption band were observed (Table S6 in the Supporting Information), indicative of different binding environments in the different zinc proteins. Differences in absorbance were also observed, indicating that different yields in radical semiquinone can be achieved depending on the nature of the binding environment.

The stability of the radical semiquinone species was assessed for the LmrR_M89X metalloproteins after 24 h incubation with **DTB-C**:**DTB-Q** by performing dialysis against Tris buffer at pH 7. Interestingly, the intensities of the **DTB-SQ** absorption bands after dialysis were similar to those before dialysis (Figure S14 in the Supporting Information). In the case of Fe(II), the 617 nm band disappeared, indicating that the Fe(III)-catecholato species was removed and only the semiquinone species remained. Moreover, for each metal ion the band at ~310 nm was still observed in the UV spectra after dialysis of the artificial protein solution (Figure S14c), which shows that the metal ions are still bound to the bpy moiety. Surprisingly, the absorption spectra did not show changes even after storage of the solution at 5 °C for 4 weeks (data no shown). These results demonstrate the high stability of **DTB-SQ** in the hydrophobic pore of artificial metalloproteins.

Spectroscopic Characterization of the Radical Semiquinone. **DTB-SQ** stabilized by the different designed LmrR mutants and in the presence of the different transition-metal ions was further characterized by magnetic (EPR) and vibrational (resonance Raman) spectroscopy. EPR spectra at room temperature showed the presence of a broad signal at g = 2.003 for every semiquinone solution, which corresponds to a radical species similar to reported by DeGrado et al. (Figure 5).[21]

Resonance Raman spectra were recorded after addition of **DTB-C**:**DTB-Q** 1:1 solution in DMSO to LmrR_V15X_Zn(II), which showed higher yields in **DTB-SQ** in comparison to LmrR_M89X_Zn(II) (Figure 6). Over time, bands appeared at 1543, 1319, 1167, and 614 cm^{-1}, which are assigned to C═C stretching of the aromatic ring, C═O stretching, C−H bending in plane, and ring breathing stretching, respectively. The observed Raman bands are different from those reported for an Fe(III)-catecholato complex, excluding that the species are metal catecholates.[22]

Resonance Raman spectra on solutions containing LmrR_M89X or LmrR_M89X_V15E_F93D in the presence of different metal ions and after 24 h incubation with **DTB-C**:**DTB-Q** 1:1 were measured (Figure S16 in the Supporting Information). The same Raman shifts as with LmrR_V15X_Zn(II) were observed for all solutions, albeit with differences in intensity. This suggests that different conversions to the semiquinone were achieved depending on the metal ion used. Moreover, the bands were still observed after dialysis (Figure S17 in the Supporting Information), corroborating the results obtained by absorption spectroscopy.

CONCLUSION

Here we have shown that by in vivo incorporation of an unnatural amino acid (bpyA), a defined metal binding environment can be created within a protein scaffold. A variety of divalent metal ions can bind with good affinity. In those cases where initially no binding was observed, e.g. with Fe(II), this could be achieved by optimizing the binding site by introducing additional ligating residues in proximity of the bpyA residue, such as aspartate, glutamate, or histidine that are found in the binding sites of natural metalloproteins. Further spectroscopic

DOI: 10.1021/acs.inorgchem.7b02073
Inorg. Chem. 2017, 56, 13293−13299

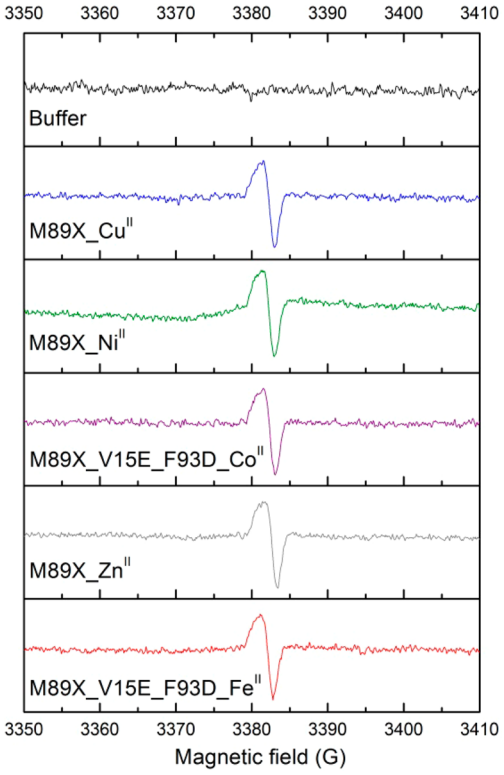

Figure 5. EPR spectra of **DTB-SQ** bound by LmrR_M89X with Cu(II), Ni(II), and Zn(II), and by LmrR_M89X_V15E_F93D with Fe(II) and Co(II), in comparison to the baseline. Absorption spectra of the corresponding solutions are presented in Figure S15 in the Supporting Information.

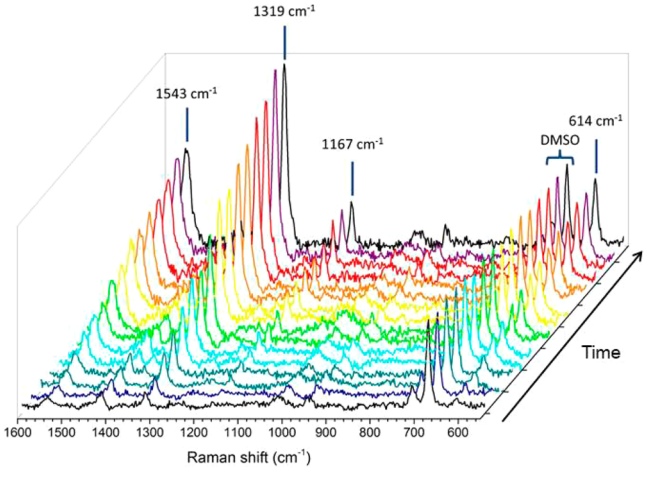

Figure 6. Resonance Raman spectra over time following addition of 30 μM monomer LmrR_V15X_Zn^{II} solution (bottom spectrum) of 20 equiv of **DTB-C**:**DTB-Q** 1:1, over 200 min (top spectrum). Excitation was at 785 nm, and spectra are baseline corrected.

analyses are required to determine the binding geometry of the different metals.

Reminiscent of natural enzymes, the artificial metalloproteins were shown to be capable of binding and stabilizing the radical semiquinone **DTB-SQ**. Binding this normally unstable species in the hydrophobic pore of LmrR results in shielding it from the aqueous environment, which normally has a detrimental effect on stability. The metal plays a key role in the binding of the radical semiquinone within the protein pocket and, hence, in its stabilization. The stabilization of radical species is the first step toward harnessing the chemistry of unstable radicals in water, potentially allowing future application in catalysis of radical reactions or one-electron-redox processes.

EXPERIMENTAL SECTION

Materials and Methods. *E. coli* strains NEB5-alpha and BL21(DE3) (New England Biolabs) were used for cloning and expression. DNA sequencing was carried out by GATC-Biotech (Berlin, Germany). Primers were synthesized by Eurofins MWG Operon (Ebersberg, Germany). Restriction endonucleases were purchased from New England Biolabs. Plasmid Purification Kit was purchased from QIAGEN. *Pfu* Turbo polymerase was purchased from Agilent. Strep-tactin columns were purchased from Iba-lifesciences. Chemicals were purchased from Sigma-Aldrich and used without further purification. The following metal salts were used: $Cu(NO_3)_2 \cdot 3H_2O$, $Zn(NO_3)_2 \cdot 6H_2O$, $Ni(NO_3)_2 \cdot 6H_2O$, $Mn(NO_3)_2 \cdot 4H_2O$, $Co(NO_3)_2 \cdot 6H_2O$, and $(NH_4)_2Fe(SO_4)_2 \cdot 6H_2O$.

All experiments are performed in freshly prepared Tris buffer pH 7 (50 mM Tris, 500 mM NaCl) at room temperature, unless otherwise specified. UPLC-MS spectra were measured on a Waters UPLC-MS instrument with C8 reversed phase column (Acquity BEH C8 1.7 μm 2.1 × 150 mm) in phosphate buffer pH 8 (50 mM NaH_2PO_4, 500 mM NaCl) with TQD detection. Exact masses of the proteins were extracted from the spectra by deconvolution using MagTran software. UV/vis absorption spectra were recorded at room temperature on a Jasco V-660 spectrophotometer. The concentration of the protein and bpyA was 30 μM in monomer in buffer pH 7 (50 mM phosphate buffer, 500 mM NaCl), unless otherwise specified. For kinetic experiments, absorbance was measured every 1 min over 900 min. Absorption maxima are ±2 nm. EPR spectra (X-band, 9.46 GHz) were recorded on a Bruker ECS106 spectrometer at room temperature. Experimental conditions: microwave frequency, 9.46 GHz; microwave power, 20 mW; 10 G field modulation amplitude; time constant 81.92 ms; scan time 83.89 s; three accumulations. Resonance Raman spectra were obtained with excitation at 785 nm using a PerkinElmer Raman station. Data were recorded and processed using Spectrum (PerkinElmer) and Spectrogryph. Samples were held in 10 mm path length quartz cuvettes.

Molecular Biology. Site-directed mutagenesis was used for preparation of all LmrR mutants. It was performed on the previously reported plasmids pET17b_LmrR_LM, pET17b_LmrR_LM_M89X, pET17b_LmrR_LM_M89X_F93D, and pET17b_LmrR_LM_M89X_F93H, according to the needed mutation.[23,27] The primers required for the mutagenesis are summarized in Table S1 in the Supporting Information. The following PCR cycles were used: initial denaturation at 95 °C for 1 min, denaturation at 95 °C for 30 s, annealing at 58−63 °C for 30 s (depending on the T_m of the particular mutant), and extension at 72 °C for 4 min 30 s. The thermal cycle was repeated 16 times. The resulting PCR product was digested with restriction endonuclease *DpnI* for 1 h at 37 °C and transformed into the *E. coli* NEB5-alpha cells. Site-directed mutagenesis for the other mutants has been previously reported.[25] In the text, the proteins have been named without the "LM" label.

Protein Expression and Purification. The plasmids pEVOL-bpyA and pET17b_LmrR_LM_X were cotransformed into *E. coli* BL21(DE3), and a single colony was used to inoculate an overnight culture of 10 mL of fresh LB medium containing 100 μg/mL of ampicillin and 34 μg/mL of chloramphenicol at 37 °C. A 2 mL portion (500× dilutions) of overnight culture was used to inoculate at 37 °C 500 mL of fresh LB medium containing 100 μg/mL of ampicillin and 34 μg/mL of chloramphenicol. When the culture reached an optical density at 600 nm of 0.8−0.9, the expression was induced with isopropyl β-D-1-thiogalactopyranoside (IPTG) (final concentration 1 mM) and L-arabinose (final concentration 0.02%), and 100 mg/L of bpyA (racemic mixture, for synthesis see ref 2) was added. Expression was done overnight at 30 °C. Cells were harvested by centrifugation (6000 rpm, JA10, 20 min, 4 °C, Beckman), resuspended in washing buffer (50 mM NaH_2PO_4, 500 mM NaCl, pH 8.0), and sonicated

DOI: 10.1021/acs.inorgchem.7b02073
Inorg. Chem. 2017, 56, 13293−13299

(70% (200 W) for 7 min (10 s on, 15 s off)). The lysed cells were incubated with DNase I (final concentration 0.1 mg/mL with 10 mM $MgCl_2$) and PMSF solution (final concentration 0.1 mM) for 30 min at 4 °C. After centrifugation (15000 rpm, JA-17, 1 h, 4 °C, Beckman), the supernatant was loaded on a Strep-Tactin column (Strep-Tactin Superflow high capacity) and incubated for 1 h at 4 °C. The column was washed with 3 × 1 CV (column volume) of resuspension buffer (same as washing buffer used before) and eluted with 6 × 0.5 CV of resuspension buffer containing 5 mM desthiobiotin. The fractions were analyzed by SDS-PAGE electrophoresis on 12% polyacrylamide SDS-Tris Tricine gel followed by Coomassie staining. The concentration of the proteins was determined by using the calculated extinction coefficient ε_{280} = 40240 M^{-1} cm^{-1} corrected for the absorbance of the bpyA. Expression yields were 2−10 mg/L of bacteria culture. Protein solutions were then dialyzed against Tris buffer (50 mM Tris, 500 mM NaCl, pH 7.0) overnight at 4 °C.

Radical Stabilization Experiments. All experiments were run at room temperature and under aerobic conditions. To a solution of 30 μM of artificial protein in 250 μL of 50 mM Tris buffer pH 7 was added 0.9 equiv of the metal salt solution (2 μL from a 3.4 mM solution in Milli-Q water). After 1 h of incubation, 5 μL of a freshly prepared 15 mM DTB-C:DTB-Q 1:1 solution in DMSO was added, and the absorption at 735 nm was recorded over 15 h. The solutions were then dialyzed overnight against 50 mM Tris buffer pH 7 at 4 °C. Absorption spectra were measured at each step of the experiment. Resonance Raman and EPR spectra were recorded at the end of the experiment.

■ ASSOCIATED CONTENT

Supporting Information

The Supporting Information is available free of charge on the ACS Publications website at DOI: 10.1021/acs.inorgchem.7b02073.

List of primers, SDS-PAGE gels, UPLC mass spectra, additional UV/vis/NIR, EPR, and resonance Raman data, and additional LmrR structure representation (PDF)

■ AUTHOR INFORMATION

Corresponding Author

*E-mail for G.R.: j.g.roelfes@rug.nl.

ORCID

Nathalie Ségaud: 0000-0002-9221-1416

Wesley R. Browne: 0000-0001-5063-6961

Gerard Roelfes: 0000-0002-0364-9564

Notes

The authors declare no competing financial interest.

■ ACKNOWLEDGMENTS

This project was supported by the European Research Council (ERC starting grant no. 280010) and The Netherlands Organisation for Scientific Research (Vici grant, 724.013.003). G.R. and W.R.B. acknowledge support from the Ministry of Education, Culture and Science (Gravity programme no. 024.001.035). J.C. acknowledges the China Scholarship Council (CSC). The authors thank Prof. P. G. Schultz (The Scripps Research Institute) for kindly providing the pEVOL plasmid for in vivo incorporation of bpyA.

■ ABBREVIATIONS

bpyA,(2,2′-bipyridin-5-yl)alanine; bpy,bipyridyl; LmrR,lactococcal multidrug resistance regulator; Tris,2-amino-2-hydroxymethyl-1,3-propanediol; EPR,electron paramagnetic resonance; DMSO,dimethyl sulfoxide

■ REFERENCES

(1) Schwizer, F.; Okamoto, Y.; Heinisch, T.; Gu, Y.; Pellizzoni, M. M.; Lebrun, V.; Reuter, R.; Köhler, V.; Lewis, J. C.; Ward, T. R. Artificial Metalloenzymes: Reaction Scope and Optimization Strategies. *Chem. Rev.* **2017**, DOI: 10.1021/acs.chemrev.7b00014.

(2) Wieszczycka, K.; Staszak, K. Artificial Metalloenzymes as Catalysts in Non-Natural Compounds Synthesis. *Coord. Chem. Rev.* **2017**, DOI: 10.1016/j.ccr.2017.06.012.

(3) Churchfield, L. A.; George, A.; Tezcan, F. A. Repurposing Proteins for New Bioinorganic Functions. *Essays Biochem.* **2017**, *61*, 245−258.

(4) Nastri, F.; Chino, M.; Maglio, O.; Bhagi-Damodaran, A.; Lu, Y.; Lombardi, A. Design and Engineering of Artificial Oxygen-Activating Metalloenzymes. *Chem. Soc. Rev.* **2016**, *45*, 5020−5054.

(5) Hyster, T. K.; Ward, T. R. Genetic Optimization of Metalloenzymes: Enhancing Enzymes for Non-Natural Reactions. *Angew. Chem., Int. Ed.* **2016**, *55*, 7344−7357.

(6) Hoarau, M.; Hureau, C.; Gras, E.; Faller, P. Coordination Complexes and Biomolecules: A Wise Wedding for Catalysis Upgrade. *Coord. Chem. Rev.* **2016**, *308*, 445−459.

(7) Heinisch, T.; Ward, T. R. Latest Developments in Metalloenzyme Design and Repurposing. *Eur. J. Inorg. Chem.* **2015**, *2015*, 3406−3418.

(8) Lewis, J. C. Metallopeptide Catalysts and Artificial Metalloenzymes Containing Unnatural Amino Acids. *Curr. Opin. Chem. Biol.* **2015**, *25*, 27−35.

(9) Pordea, A. Metal-Binding Promiscuity in Artificial Metalloenzyme Design. *Curr. Opin. Chem. Biol.* **2015**, *25*, 124−132.

(10) Drienovská, I.; Roelfes, G. Artificial Metalloenzymes for Asymmetric Catalysis by Creation of Novel Active Sites in Protein and DNA Scaffolds. *Isr. J. Chem.* **2015**, *55*, 21−31.

(11) Zastrow, M. L.; Pecoraro, V. L. Designing Functional Metalloproteins: From Structural to Catalytic Metal Sites. *Coord. Chem. Rev.* **2013**, *257*, 2565−2588.

(12) Deuss, P. J.; den Heeten, R.; Laan, W.; Kamer, P. C. J. Bioinspired Catalyst Design and Artificial Metalloenzymes. *Chem. - Eur. J.* **2011**, *17*, 4680−4698.

(13) Zhao, M.; Wang, H.-B.; Ji, L.-N.; Mao, Z.-W. Insights into Metalloenzyme Microenvironments: Biomimetic Metal Complexes with a Functional Second Coordination Sphere. *Chem. Soc. Rev.* **2013**, *42*, 8360.

(14) Liu, J.; Meier, K. K.; Tian, S.; Zhang, J.; Guo, H.; Schulz, C. E.; Robinson, H.; Nilges, M. J.; Münck, E.; Lu, Y. Redesigning the Blue Copper Azurin into a Redox-Active Mononuclear Nonheme Iron Protein: Preparation and Study of Fe(II)-M121E Azurin. *J. Am. Chem. Soc.* **2014**, *136*, 12337−12344.

(15) Cook, S. A.; Borovik, A. S. Molecular Designs for Controlling the Local Environments around Metal Ions. *Acc. Chem. Res.* **2015**, *48*, 2407−2414.

(16) Simmons, T. R.; Berggren, G.; Bacchi, M.; Fontecave, M.; Artero, V. Mimicking Hydrogenases: From Biomimetics to Artificial Enzymes. *Coord. Chem. Rev.* **2014**, *270*−*271*, 127−150.

(17) Span, E. A.; Suess, D. L. M.; Deller, M. C.; Britt, R. D.; Marletta, M. A. The Role of the Secondary Coordination Sphere in a Fungal Polysaccharide Monooxygenase. *ACS Chem. Biol.* **2017**, *12*, 1095−1103.

(18) McQuarters, A. B.; Speelman, A. L.; Chen, L.; Elmore, B. O.; Fan, W.; Feng, C.; Lehnert, N. Exploring Second Coordination Sphere Effects in Nitric Oxide Synthase. *JBIC, J. Biol. Inorg. Chem.* **2016**, *21*, 997−1008.

(19) Sever, M. J.; Wilker, J. J. Visible Absorption Spectra of Metal-Catecholate and Metal-Tironate Complexes. *Dalt. Trans.* **2004**, 1061−1072.

(20) Pierpont, C. G.; Lange, C. W.; Karlin, K. D. The Chemistry of Transition Metal Complexes Containing Catechol and Semiquinone Ligands. *Prog. Inorg. Chem.* **1994**, *41*, 331−442.

(21) Ulas, G.; Lemmin, T.; Wu, Y.; Gassner, G. T.; DeGrado, W. F. Designed Metalloprotein Stabilizes a Semiquinone Radical. *Nat. Chem.* **2016**, *8*, 354−359.

DOI: 10.1021/acs.inorgchem.7b02073
Inorg. Chem. 2017, 56, 13293−13299

(22) Horsman, G. P.; Jirasek, A.; Vaillancourt, F. H.; Barbosa, C. J.; Jarzecki, A. A.; Xu, C.; Mekmouche, Y.; Spiro, T. G.; Lipscomb, J. D.; Blades, M. W.; et al. Spectroscopic Studies of the Anaerobic Enzyme−Substrate Complex of Catechol 1,2-Dioxygenase. *J. Am. Chem. Soc.* **2005**, *127*, 16882−16891.
(23) Siegbahn, P. E. M. The Catalytic Cycle of Catechol Oxidase. *JBIC, J. Biol. Inorg. Chem.* **2004**, *9*, 577−590.
(24) Ramsden, C. A.; Riley, P. A. Tyrosinase: The Four Oxidation States of the Active Site and Their Relevance to Enzymatic Activation, Oxidation and Inactivation. *Bioorg. Med. Chem.* **2014**, *22*, 2388−2395.
(25) Drienovská, I.; Rioz-Martinez, A.; Draksharapu, A.; Roelfes, G. Novel Artificial Metalloenzymes by in Vivo Incorporation of Metal-Binding Unnatural Amino Acids. *Chem. Sci.* **2015**, *6*, 770−776.
(26) Bos, J.; Browne, W. R.; Driessen, A. J. M.; Roelfes, G. Supramolecular Assembly of Artificial Metalloenzymes Based on the Dimeric Protein LmrR as Promiscuous Scaffold. *J. Am. Chem. Soc.* **2015**, *137*, 9796−9799.
(27) Bos, J.; García-Herraiz, A.; Roelfes, G. An Enantioselective Artificial Metallo-Hydratase. *Chem. Sci.* **2013**, *4*, 3578.
(28) Bos, J.; Fusetti, F.; Driessen, A. J. M.; Roelfes, G. Enantioselective Artificial Metalloenzymes by Creation of a Novel Active Site at the Protein Dimer Interface. *Angew. Chem.* **2012**, *124*, 7590−7593.
(29) Bersellini, M.; Roelfes, G. Multidrug Resistance Regulators (MDRs) as Scaffolds for the Design of Artificial Metalloenzymes. *Org. Biomol. Chem.* **2017**, *15*, 3069−3073.
(30) Xie, J.; Schultz, P. G. An Expanding Genetic Code. *Methods* **2005**, *36*, 227−238.
(31) Madoori, P. K.; Agustiandari, H.; Driessen, A. J. M.; Thunnissen, A.-M. W. H. Structure of the Transcriptional Regulator LmrR and Its Mechanism of Multidrug Recognition. *EMBO J.* **2009**, *28*, 156−166.
(32) Drienovská, I.; Alonso-Cotchico, L.; Vidossich, P.; Lledós, A.; Maréchal, J.-D.; Roelfes, G. Design of an Enantioselective Artificial Metallo-Hydratase Enzyme Containing an Unnatural Metal-Binding Amino Acid. *Chem. Sci.* **2017**, *8*, 7228−7235.
(33) Koehntop, K. D.; Emerson, J. P.; Que, L. The 2-His-1-Carboxylate Facial Triad: A Versatile Platform for Dioxygen Activation by Mononuclear Non-Heme iron(II) Enzymes. *JBIC, J. Biol. Inorg. Chem.* **2005**, *10*, 87−93.
(34) Zastrow, M. L.; Pecoraro, V. L. Designing Hydrolytic Zinc Metalloenzymes. *Biochemistry* **2014**, *53*, 957−978.
(35) Meyer, T. Photochemistry of Metal Coordination Complexes: Metal to Ligand Charge Transfer Excited States. *Pure Appl. Chem.* **1986**, *58*, 1193−1206.
(36) Mason, S. F. The Electronic Spectra and Optical Activity of Phenanthroline and Dipyridyl Metal Complexes. *Inorg. Chim. Acta, Rev.* **1968**, *2*, 89−109.
(37) Imperiali, B.; Fisher, S. L. (S)-.alpha.-Amino-(2,2′-bipyridine)-6-Propanoic Acid: A Versatile Amino Acid for de Novo Metalloprotein Design. *J. Am. Chem. Soc.* **1991**, *113*, 8527−8528.
(38) Zhang, C.; Janiak, C. Six-Coordinated Zinc Complexes: [Zn(H2O)4(phen)] (NO3)2·H2O and [ZnNO3(H2O)(bipy)-(Him)]NO3 (phen = 1,10-Phenanthroline, bipy = 2,2?-Bipyridine, and Him = imidazole). *J. Chem. Crystallogr.* **2001**, *31*, 29−35.
(39) Jovanovic, S. V.; Konya, K.; Scaiano, J. C. Redox Reactions of 3,5-Di-Tert-Butyl-1,2-Benzoquinone. Implications for Reversal of Paper Yellowing. *Can. J. Chem.* **1995**, *73*, 1803−1810.
(40) Mialane, P.; Tchertanov, L.; Banse, F.; Sainton, J. Jean-Jacques Girerd. Aminopyridine Iron Catecholate Complexes as Models for Intradiol Catechol Dioxygenases. Synthesis, Structure, Reactivity, and Spectroscopic Studies. *Inorg. Chem.* **2000**, *39*, 2440−2444.
(41) Dhanalakshmi, T.; Bhuvaneshwari, M.; Palaniandavar, M. Iron(III) Complexes of Certain Meridionally Coordinating Tridentate Ligands as Models for Non-Heme Iron Enzymes: The Role of Carboxylate Coordination. *J. Inorg. Biochem.* **2006**, *100*, 1527−1534.
(42) Bruijnincx, P. C. A.; Lutz, M.; Spek, A. L.; Hagen, W. R.; Weckhuysen, B. M.; van Koten, G.; Gebbink, R. J. M. K. Modeling the 2-His-1-Carboxylate Facial Triad: Iron−Catecholato Complexes as Structural and Functional Models of the Extradiol Cleaving Dioxygenases. *J. Am. Chem. Soc.* **2007**, *129*, 2275−2286.

DOI: 10.1021/acs.inorgchem.7b02073
Inorg. Chem. 2017, 56, 13293−13299